The Crystallisation of Glasses Based on Eutectic Compositions in the System Li$_2$O - Al$_2$O$_3$ - SiO$_2$

Part 1 *Lithium Metasilicate* — β-*Spodumene*

T. I. BARRY, D. CLINTON, L. A. LAY, R. A. MERCER, R. P. MILLER
National Physical Laboratory, Teddington, Middlesex, UK

Structural transformations have been studied in glasses related in composition to the binary eutectic between lithium metasilicate and β-spodumene. Crystallisation processes and changes in microstructure during the controlled heating of the glasses have been followed using X-ray diffraction, electron microscopy, high temperature microscopy, thermal analysis and electron spin resonance spectroscopy.

The influence exerted by titanium dioxide on the phase relationships, crystal growth rates and micromorphology of the polycrystalline products of heat-treatment has been investigated and the findings used as a basis for proposals on the rôle of TiO$_2$ during nucleation and crystal growth.

1. Introduction

Because of their relevance to glass-ceramic technology, crystallisation studies on glasses based on the ternary system Li$_2$O–Al$_2$O$_3$–SiO$_2$ have formed the basis of many publications over the last few years [1-3]. The importance of the system rests mainly on the occurrence within it of stability fields of the framework silicates β-spodumene (Li$_2$O.Al$_2$O$_3$.4 SiO$_2$) and related solid solutions, all of which have low expansion coefficients.

In spite of the attention that has been given to the subject in general and to the Li$_2$O–Al$_2$O$_3$–SiO$_2$ system in particular, there are many basic aspects of crystal nucleation and growth mechanisms which have still to be resolved.

A complication commonly noted in glass devitrification studies is the initial formation and subsequent transformation of metastable phases. These frequently have a simple structure which is unrelated to the structure of the final stable crystals. A study of the course of such changes towards equilibrium in terms of the composition, structure, size and distribution of the crystal phases during heat-treatment is essential to an understanding of the glass-ceramic process and is a general objective of the present study on the systems chosen.

The origin of metastable structures must relate to the short range order, which already exists in the glass, and which arises from the local interactions of the cations with their environment. Such interactions are of fundamental importance as precursors to compound formation and chemical differentiation which may lead to glass-in-glass separation. This latter phenomenon has been observed in many glasses on heating and has been considered by many workers [4-7] to be essential for the nucleation of fine-grained crystallisation. On this model the function of TiO$_2$, for example, is to induce this pre-crystallisation microphase separation. Others [6-8] have held that the effective nuclei are small crystallites ($\sim$ 20 to 100 Å diameter) of titanium compounds such as TiO$_2$ itself or titanates. The conflict of opinion on these issues is still unresolved and a specific aim of this work is the clarification of the mode of action of TiO$_2$ in modifying crystallisation processes. However, the function of TiO$_2$ is likely to be dependent on

glass composition, so our conclusions should not be taken as invalidating previously held opinions for totally different compositions.

Any new investigation in the Li_2O–Al_2O_3–SiO_2 system was considered likely to serve a useful purpose only if it related to a region in the phase diagram which had not been examined in detail by other workers, but which nevertheless might be of both fundamental and practical interest. For this reason choice fell on the two binary eutectic points lithium metasilicate–β-spodumene [9], and lithium metasilicate–β-eucryptite [10].

In structurally simpler systems, such as metallic alloys and mixtures of simple inorganic salts or oxides, eutectic solidification gives rise to characteristic microstructures which can confer special properties, notably strength, on the crystallised body. The fine-grained, highly inter-connected nature of this type of crystallisation is caused by the simultaneous growth of two (or more) phases at equilibrium and it is known that eutectic crystallisation requires a lower degree of undercooling and proceeds more rapidly than does the crystallisation of the single components. Thus the characteristic behaviour of eutectics would at first sight be highly desirable in the con-text of a glass-ceramic process but the relevance to silicate glass-forming systems where non-equi-librium crystallisation is known to be prevalent is less clear. The possibility, however, that some eutectic crystal growth mechanisms [11] might be operative during the crystallisation of glasses based on the two eutectic points in the Li_2O–Al_2O_3–SiO_2 system, stimulated this present study which is reported and discussed in two parts.

2. Experimental
2.1. Glass Compositions
The detailed formulations are given in table I.

Titanium dioxide additions were made in two arbitrary ways.
(i) 4 moles and 7.5 moles of TiO_2 respectively were added in excess of the appropriate stoichio-metries of $Li_2O : Al_2O_3 : SiO_2$, these being expressed on a 100 mole % basis.
(ii) The same molar quantities were added on a TiO_2 for SiO_2 substitutional basis.

Although strictly requiring representation on a tetrahedral figure, the compositions relevant to the present study are indicated in fig. 1 which is the ternary system redrawn on a molar basis from data available in the literature.

Small quantities (0.2 wt. %) of V_2O_5 or Cr_2O_3
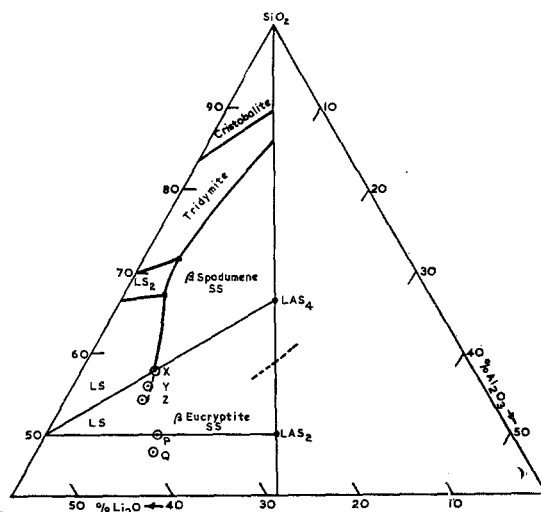
Figure 1 Phase Diagram Li_2O–Al_2O_3–SiO_2 (mole %). Primary phase field data after Roy and Osborn [9], and Murthy and Hummel [10].
$X = LS$–β-LAS_4 eutectic (G 66) and L:A:S ratio in G 67 and G 69, $Y =$ L:A:S ratio in G 68, $Z =$ L:A:S ratio in G 70, P and Q refer to compositions to be the subject of part 2 of this work.

TABLE I Glass compositions.

| Glass no. | Li₂O | | Al₂O₃ | | SiO₂ | | TiO₂ | |
	wt %	mole* ratio	wt %	mole* ratio	wt %	mole* ratio	wt %	mole* ratio
G 66	19.46	34.47	14.96	7.76	65.68	57.76	—	—
G 67	18.35	34.47	14.10	7.76	61.84	57.76	5.69	4.00
G 68	19.17	35.91	14.74	8.09	60.14	56.0	5.95	4.17
G 69	17.48	34.47	13.44	7.76	58.91	57.76	10.17	7.5
G 70	18.93	37.26	14.55	8.39	55.51	54.34	11.01	8.11

*L + A + S = 100.

were added to some batches of the glasses for the purposes of the electron spin resonance studies.

2.2. Glass Preparation
2.2.1. Reagents
The reagents were aluminium oxide 99.99% Al_2O_3, lithium carbonate 99.99% Li_2CO_3, titanium dioxide 99.99% TiO_2, all Johnson Matthey Grade II reagents; crushed fused quartz 99.99% SiO_2, Thermal Syndicate Ltd.

2.2.2. Firing Procedure
Batches of approximately 150 g were prepared by fusing the appropriate mix in a platinum dish at 1450° C for 2 h. The melt was poured into a water cooled platinum dish and the glass crushed and ground. This melt quench procedure was carried out three times to ensure homogeneity. The glass compositions were confirmed by chemical analysis.

Specimens of glass for subsequent heat-treatment were prepared in the form of buttons 1.5 cm diameter × 0.3 cm, by pressing 1 g quantities of melt between vitreous carbon plates.

2.3. Differential Thermal Analysis (dta)
Heat effects accompanying the transformations were recorded on a Stanton Standata 6-25 instrument operated at 10° C/min. Specimens of mass 0.3 g were melted into the platinum sample holders at 1450° C and were then air-quenched to room temperature.

The phase changes responsible for the heat effects were inferred by heat-treatment of glass buttons in a furnace programmed to rise at 10° C/min, and removal of specimens at appropriate temperatures for X-ray diffraction analysis.

Use was also made of a hot-stage microscope/ micro dta technique [12]. The full results of these studies will be reported separately.

2.4. Heat Schedules
To standardise thermal histories the glass discs were placed in a cold muffle furnace, the temperature of which was programmed to rise at a constant rate of 10° C/min to the required holding temperature. The furnace could be programmed for two consecutive heat-treatments on the same glass. At the completion of a heat sequence the furnace was switched off and the samples were cooled in the furnace.

Although to some extent arbitrary, the choice of temperatures was guided by results from

thermal analysis. Changes in the vicinity of the glass transformation temperature (T_g) and in the temperature region for very slow crystallisation were studied at 520 and 580° C and influences of such preheating on later crystallisation were investigated at 700 and 900° C.

2.5. Electron Microscopy
A JEM7 instrument was used to examine replicas taken from fracture surfaces of specimens and also to study, in transmission, thin sections cut with a diamond knife in an ultramicrotome (LKB).

Most replicas were taken using a single stage technique involving the simultaneous deposition of a carbon/platinum film on the surface from which the replica was floated onto a copper grid. Before replication, the specimens were either fractured and then etched by HF (e.g. 0.5% for 5 sec) or fractured in vacuum with no exposure to air. An externally operated jig was devised for breaking the glass within a standard evaporating unit.

Occasionally, use was made of a two-stage replication procedure in which a carbon layer was deposited onto a plastic impression of the surface. This frequently enabled transmission electron micrographs to be made of the crystalline regions which sometimes adhered to the plastic. These micrographs provided useful information on the nature and orientation of the phases.

2.6. X-ray Diffraction
Powder photographs were produced in a Phillips 11.4 cm camera using Cu $K\alpha$ radiation.

2.7. Electron Spin Resonance (esr)
Unless otherwise stated measurements were made at room temperature in a Decca spectrometer operating at a fixed microwave frequency of 9270 mc/s.

2.8. Density Measurement
The specific gravities of small fragments were determined using a Techne density gradient column.

2.9. Nomenclature
An abbreviated form of representing phase compositions will be used where L = Li_2O; A = Al_2O_3; S = SiO_2; T = TiO_2; for example Li_2TiSiO_5 becomes LTS. β-eucryptite solid solutions will be referred to as β-eucryptite

because of deviations in SiO_2 content from the nominal composition LAS_2.

3. Results
3.1. Transformations During Programmed Heating

Differential thermal analysis and hot-stage microscopy enabled specimens to be examined during heating while X-ray diffraction and optical and electron microscopy on quenched specimens helped to establish the sequence of the structural transformations and their association with the thermal effects.

A summary of the data is given in table II, selected examples of dta traces are illustrated in fig. 2, and table III gives the crystallochemical characteristics of all the phases encountered in the complete study of these systems. All the dta traces were characterised by a pronounced exothermic peak occurring at temperatures 100 to 200° C above T_g, the glass transition temperature. T_g was registered by a sharp fall in the base line corresponding to the increase in specific heat.
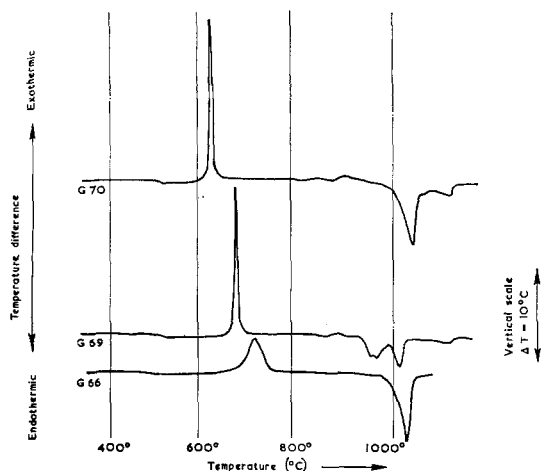
Figure 2 Thermograms of glasses G 66, G 69 and G 70. Heating rate 10° C/min. Sample weight 0.3 g.

In every case the exotherms were associated with the simultaneous crystallisation of LS and β-eucryptite, but variations in the temperature and the temperature span of the exotherms indicated that incorporation of TiO_2 in the glasses modified the crystallisation kinetics (cf.

section 3.2.4). The sequence of crystallisation of LT, which appeared without any detectable heat effect, also changed with TiO_2 content. In G 70 the generation of LT preceded the exotherm, whereas in other titanium containing glasses LT invariably crystallised after LS and β-eucryptite.

The examination of specimens prepared by various heat treatments of glasses G 66 to 69 showed that the eucryptite and lithium metasilicate were intimately associated in spherulitic (figs. 3a and 3b) or biconical (fig. 4) polycrystalline growth units, whose dendritic internal structure is described more fully later. From this exploratory study it was concluded that TiO_2 addition influenced the morphology, number, and rate of growth of the crystalline units and increased the proportion of slower growing biconical crystallites. Although the term dendrite will be used when referring to these, it is worth noting that their single crystal character to be described later, makes them analogous to the hedrites found in polymer systems [14].

In G 66 to 68 the crystallites grew rapidly and impinged during the exothermic effect but, in spite of the fine-grained internal structure of the growth units, the crystallised products were coarse-grained and cracked bodies, which contained voids. In G 69, the nucleation density was much higher and the crystallites were consequently smaller; voids were still present however. Although crystallisation in G 70 was very fine-grained, the product was very fragmented and was usually split into many layers.

In order to gain an understanding of nucleation phenomena preceding crystal growth and of the morphology, internal structure, growth rate and orientation relationships between developing phases, more detailed studies were made under isothermal conditions.

3.2. Transformations During Isothermal Heating
3.2.1. Phase Changes G 66 to 69

The crystal phases present after heat-treatment of the glasses are set out in table IV together with specific gravity data and a general description of the products.

For all compositions the major phases resulting from heating at temperatures up to 700° C were β-eucryptite and LS. The first phase to be detected by X-ray diffraction was always β-eucryptite; the pattern for LS was initially less well defined. However, it was qualitatively established from esr evidence that LS was
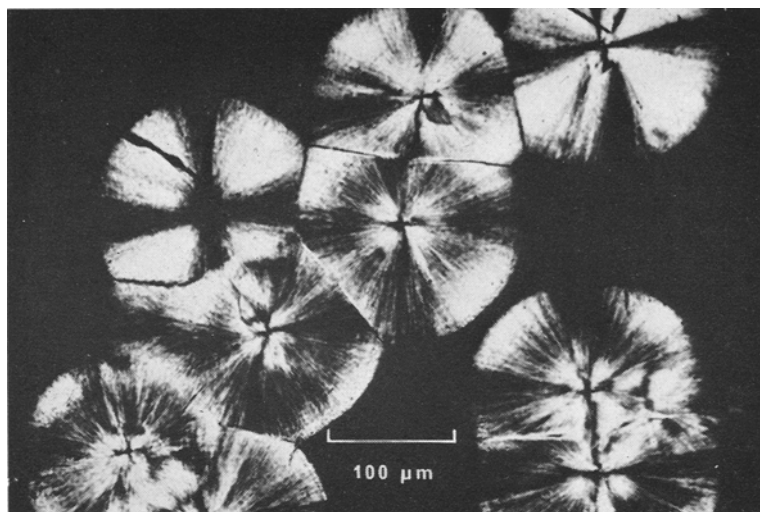
(a)
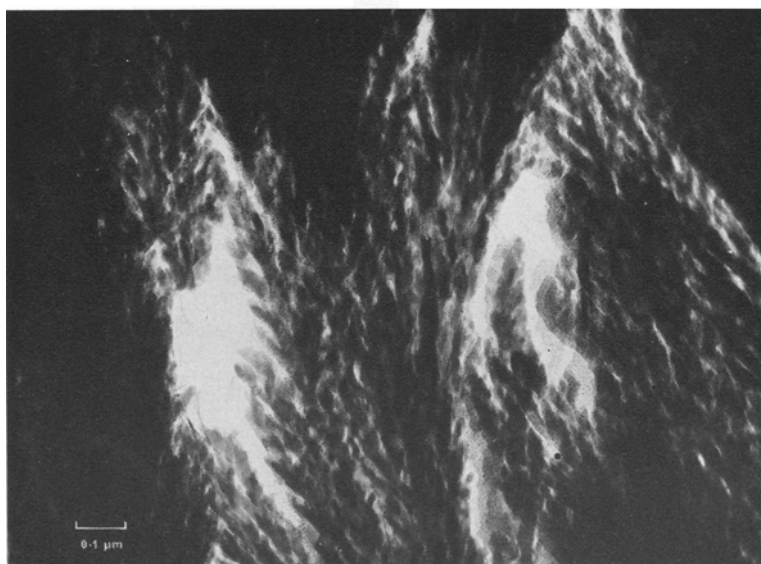
(b)

Figure 3(a) Optical micrograph of composite spherulites of LS and β-eucryptite, grown in G66 and viewed in thin section between crossed polarisers. (b) Extraction replica showing internal structure of the spherulites. The etching treatment (5 secs; $\frac{1}{2}$% HF) prior to replication selectively leached away LS. The figure shows the skeletal filaments of β-eucryptite.

present at least in a rudimentary form, during the early stages of crystallisation of G 66. V^{4+} ions present in the glasses, become preferentially sited in the LS structure during crystallisation and this change of environment was detected by the accompanying spectral changes (fig. 5). This

point and other applications of esr to glass crystallisation studies have been more fully discussed elsewhere [15].

In compositions G 67 to 69 the LT phase was developed only in specimens heated at 700° C or higher temperatures. For these specimens the

600
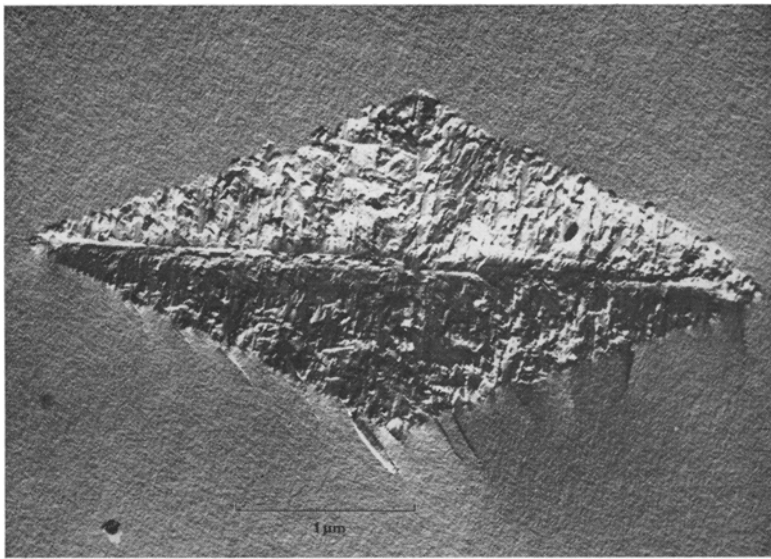
Figure 4 Dendrite of **LS** and β-eucryptite crystallising from **G 69** at 580° C. Replica from surface fractured in vacuum.

TABLE II Transformations during dta

Glass	T_g ° C ($\pm$ 10° C)	Exothermic temperature span ° C	Crystallisation temperatures of the phases (X-ray detection) $\pm$ 20° C		
			β-eucryptite	LS	LT
G 66	470	610–790	620	670	—
G 67	480	650–790	650	680	730
G 68	480	630–760	640	680	720
G 69	500	670–730	670	680	700
G 70	500	600–660	600	650	600

Sample weight 0.3 g; heating rate 10° C/min.

TABLE III Crystallographic data.

Phase and reference	Composition (nominal or stable range)	Crystal class	Unit cell
β-eucryptite (ASTM 17–533)	LAS_2 to LAS_3	hexagonal	$[a = 5.18$ to $5.31]^*$ $[c = 5.38$ to $5.58]$
β-spodumene (ASTM 13–251)	LAS_3 to LAS_7	tetragonal	$a = 7.483$ to 7.558 $c = 9.000$ to 9.172
Lithium metasilicate (ASTM 15–519)	LS	orthorhombic	$a = 5.43$ $b = 9.41$ $c = 4.66$
Lithium titanium silicate (ASTM 13–268)	LTS	tetragonal	$a = 6.44\dagger$ $c = 4.40$
Lithium aluminium oxide [13]	LA	tetragonal	$a = 5.169$ to 5.074^* $c = 6.268$ to 6.339^*
Lithium titanate	LT	cubic	$a = 8.28$
Lithium titanate (ASTM 8–249)	LT	monoclinic	$a = 5.05\ b = 8.76$ $c = 9.68\dagger\ \beta = 100°$
Hexagonal phase, LA		hexagonal?	$[a = 3.07$ to $3.09]^*$ $[c = 4.92$ to $4.86]$

*Information from the present study.   †Correction to reference.

601

LT X-ray diffraction pattern, indexed on a cubic cell with $a = 8.28$ Å, had a strong 311 reflection typical of spinel structures. The appearance of LT in G 69 could be entirely suppressed by previous heat treatment at 580° C for 20 h or
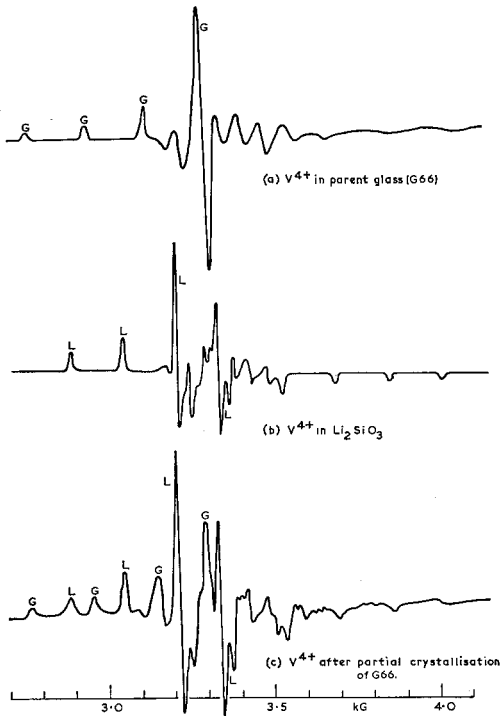
Figure 5 ESR spectra of V^{4+} in G 66, Li_2SiO_3 and G 66 after partial crystallisation. Features marked G and L are characteristic of V^{4+} in the glass and LS respectively.

more. Neither the X-ray diffraction lines nor the characteristic esr spectra of Fe^{3+} and Cr^{3+} in the LT phase could be detected after this heat-treatment, which brings about the complete volume transformation of the glass into dendrites differing in their structure from those produced at higher temperature (cf. section 3.2.6). The same heat treatment lowered the intensity of the X-ray pattern of LS relative to that of β-eucryptite.

The differences in dendrite structure described later, relate to the size and orientation of the crystallites in the dendrites. It will be argued in the discussion that there is a cause and effect relationship between this change in micro-structure and the suppression of LT formation and that these findings provide an important clue

602

to the rôle of Ti^{4+} ions in modifying nucleation and growth processes.

3.2.2. Structure of the Glasses and Products (G 66 to 69)

Carbon replicas from etched fracture surfaces and transmission micrographs from thin sections of all the quenched glasses were completely featureless (fig. 6). Replicas of specimens
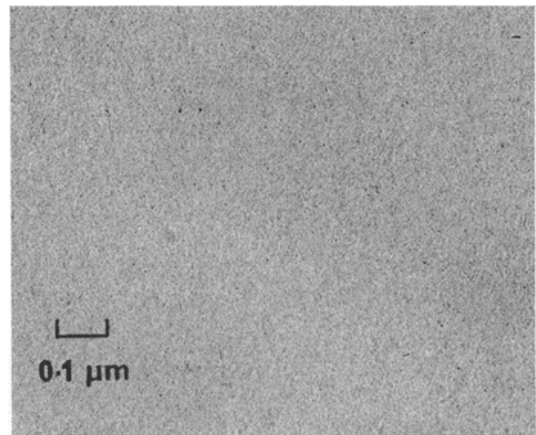
Figure 6 Featureless replica typical of all quenched glasses G 66 to 70. Replica from surface fractured in vacuum.

fractured in vacuum showed microgranularity extending over regions of 30 to 100 Å diameter but since similar replicas were produced from an α-quartz crystal conchoidally fractured in the same way, the significance of the apparent microgranularity in terms of a chemically differentiated structure in the glass was discounted. At no stage before or during the growth of crystals in these glasses was glass-in-glass separation observed.

No microstructural changes occurred with heat-treatment at 520° C but at 580° C crystallisation started with the slow appearance and development of spherulites or dendrites, the size, shape and number of which depended on the TiO_2 content. In G 66, 67 and 68 increase of temperature to 700° C caused a rapid growth of the spherulites of β-eucryptite and LS until they impinged with a final diameter of 100 to 400 μm. This size was independent of pretreatment of the specimens at 580° C, a clear indication that such preheating was ineffective in producing a useful

TABLE IV Thermal history—phase data

Heat-treatment	G 66			G 67			G 68			G 69			G 70		
	Phases	SG	Appearance	Phases	SG	Appearance	Phases	SG	Appearance	Phases	SG	Appearance	Phases	SG	Appearance
520°/16 h	—	2.398	clear glass	—	2.453	clear glass	—	2.458	clear glass	—	2.505	clear glass	LT(mw)	2.518	faint opalescence, coherent
580°/3 h	β-euc(w)	2.398	,,	β-euc(vw)	2.450	,,	β-euc(vw)	2.455	,,	β-euc(vw)	2.500	faint opalescence	β-euc(s) LS(vw) LT(mw) Hex phase (w)	2.549	fragmented opalescent
700°/3 h	β-euc (s) LS(s)	2.462	crazed, coarsely crystalline, contains visible voids	β-euc(s) LS(s)	2.498	crazed, coarsely crystalline, contains visible voids	β-euc(s) LS(s)	2.498	crazed, coarsely crystalline, contains visible voids	β-euc(s) LS(s) LT(w)	2.530	coherent opaque	β-euc(s) LS(s) LT(mw)	2.542	fragmented opaque
520°/16 h — 700°/3 h	β-euc(s) LS(s)	2.466	,,	β-euc(s) LS(s) LT(vw)	2.497	,,	β-euc(s) LS(s)	2.500	,,	β-euc(s) LS(s) LT(w)	2.510	,,	β-euc(s) LS(s) LT(w)	2.548	,,
580°/3 h — 700°/3 h	β-euc(s) LS(s)	2.463	,,	β-euc(s) LS(s)	2.502	,	β-euc(s) LS(s)	2.498	,,	β-euc(s) LS(s) LT(mw)	2.510	,	β-euc(s) LS(s) LT(vm)	2.549	,,
1000°/12 h	LS(s) β-LAS₄(s)	2.434	,,	LS(s) LTS(m) β-LAS₄(s)	2.488	,,	LS(s) LTS(m) β-LAS₄(s)	2.501	,,	LS(s) LTS(s) β-LAS₄(s)	2.540	,,	β-euc(s) LS(s) LTS(s)	2.553	,,

increase in the nuclei concentration beyond the range 10^4 to 10^6 per cc.

However, this was not the case for G 69, in which thermally activated nucleation over the temperature range 520 to 580° C could be inferred from a comparison of the electron micrographs of the products crystallised at 700° C. These showed that finer grained bodies with a greater number of dendritic crystals resulted from preheating. A systematic study, described later, showed that the optimum temperature for nucleation was approximately 535° C.

The products from the heat-treatments at 700° C were not satisfactory materials. All contained voids as shown by microscopic examination and by the difference between the density of large and small pieces. The origin of void formation is not yet clear. The products increased in opacity with increasing TiO_2 content.

3.2.3. Phase and Structural Changes in G 70

G 70 differed from the other glasses in that LT was the first phase to crystallise. Replication and thin section electron microscopy of this glass heated at 520° C for 16 h showed (fig. 7) that a uniform dispersion of crystallites, ~ 250 Å in size, had grown at a volume concentration of $4 \times 10^{15}/cm^3$. X-ray and electron diffraction con-firmed these to be LT. During more prolonged heating at 520°C (24 h) β-eucryptite progress-ively developed as 1 to 2 μm sized platy crystals, which became distributed through the glass at a volume concentration of $\sim 2 \times 10^{12}/cm^3$. Samples heated in this way broke up on cooling. Both transmission and replica electron micro-graphs (cf. fig. 8) showed that the nucleation of β-eucryptite on LT, if it occurred at all, was inefficient.

When heated at higher temperatures than 520° C, specimens of G 70 broke up either during heating or cooling. This prevented an adequate study of their microstructure in relation to the crystal phases present. These include the tran-sient hexagonal phase (table III) which is prob-ably a structural modification of LA. This will be discussed more fully elsewhere. The explanation of the different crystallisation behaviour of G 70 from the other glasses will be discussed later in terms of constitutional differences. The following sections describe work aimed at a fuller under-standing of nucleation and crystallisation rates and of the internal structure of dendrites and spherulites in G 66 to 69.

3.2.4. Crystallisation Kinetics of Growth Units

In G 66 to 68 the crystal growth units were spherulitic, a typical section being shown in
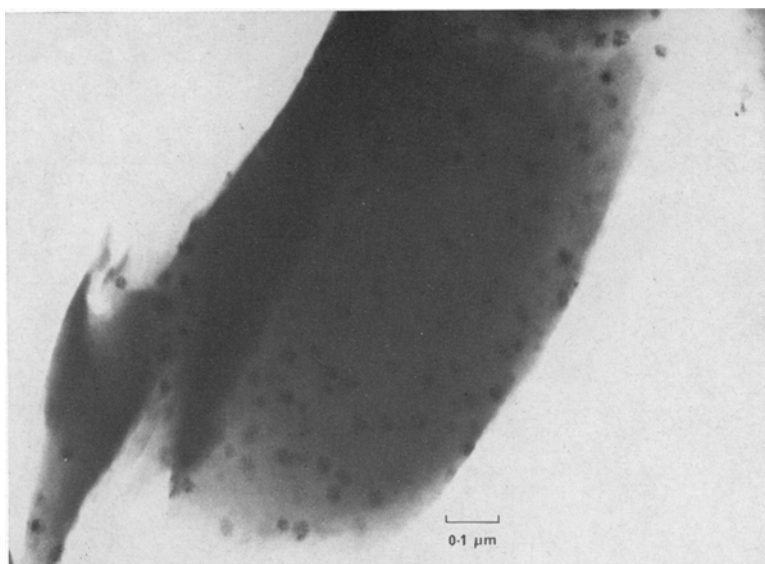
Figure 7 Transmission electron micrograph of a thin section of G 70 heated at 520° C for 16 h showing crystallites of LT.

604
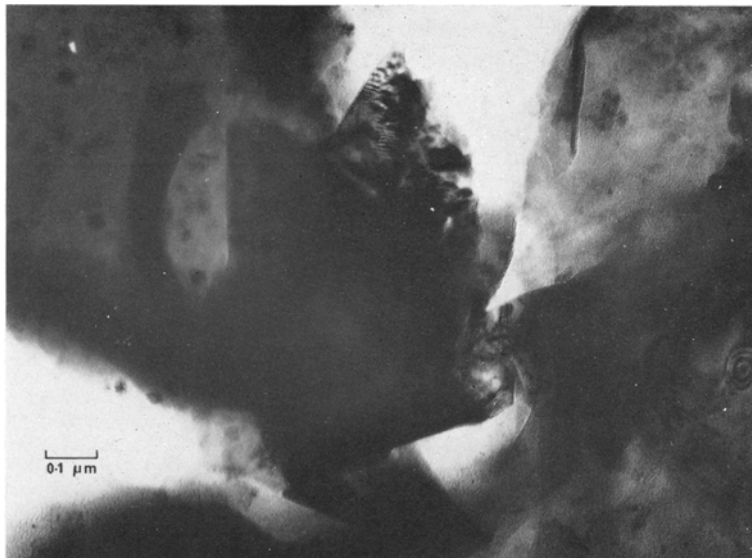
Figure 8 Transmission electron micrograph of a thin section of G 70 heated at 520° C for 24 h showing irregular development of β-eucryptite, which is seen as striped zones of diffraction contrast. LT shows up as smaller particles (cf. fig. 7).

fig. 3. Growth rate data were derived from a series of optical micrographs taken over timed intervals during isothermal heating within the temperature range 570 to 650° C. It was established that the initial radial growth rate was constant, a result typical of spherulitic growth in other silicate glass and organic polymer systems, and one which indicates that the growth mechanisms are controlled by processes at the interface rather than by bulk diffusion.

A noteworthy finding in all three glasses was a kinetic arrest of the growing spherulites. The effect is illustrated by data relating to G 66 shown in fig. 9. In no case were any heterogeneities observed at the spherulite-glass interface which could account for the temporary reduction in growth rate although it was noted that only after the kinetic arrest was LS detectable in the X-ray powder diffraction patterns. However, the characteristic spectrum of V^{4+} (cf. fig. 5) in LS became evident from the beginning of spherulite growth. A plot of the intensity of this spectrum against the duration of heat treatment paralleled the growth curve of the spherulites. Thus esr confirmed the reality of the arrest and prevented the erroneous conclusion that this arrest was due to a delayed formation of LS. It may be, however, that the modification of the growth rates was associated with the forma-

tion of larger LS crystallites which then became partially coherent with the β-eucryptite crystallites (see section 3.2.6).

In G 69 it was found that both the long and short axes of the dendritic crystals grew linearly with time. The growth rate data and derived activation energies relating to the initial stages of crystallisation in G 66 to 69 are recorded in fig. 10.

The crystallisation characteristics of G 70 did not permit the determination of growth rate data.

3.2.5. Rate of Nucleation

The rate of nucleation could be studied systematically only in G 69. In G 66 to 68 preheating had very little effect on nucleation density and in G 70 crystallisation was too rapid for convenient observation of the rate of nucleation.

Specimens of G 69 were heated in the normal way at 10° C/min to the nucleation temperature in the range 515 to 580° C and, after a measured time, the temperature was raised at the same rate to 615° C in order to develop crystal growth on the nuclei. The time and temperature for crystal development was carefully controlled in order that the dendrites so formed should fall within a small size range around 2.5 μm. The

605
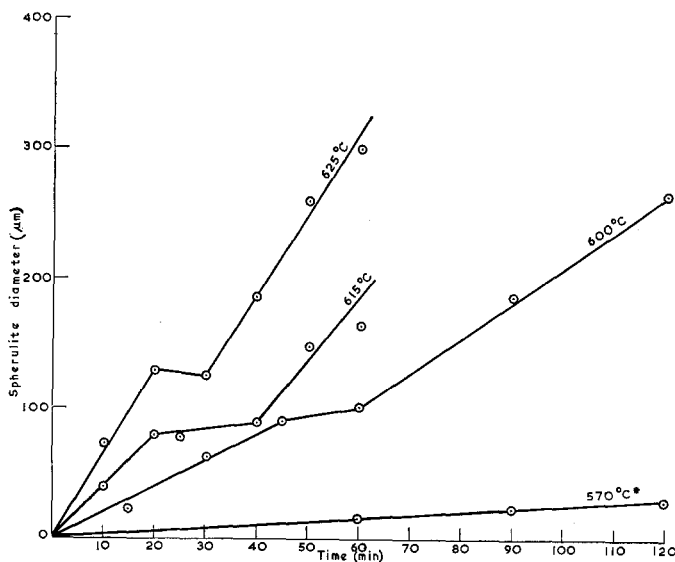
Figure 9 Kinetics of spherulite growth in G 66. At 570° C the kinetic arrest occurred when the spherulite diameter reached 36 μm.
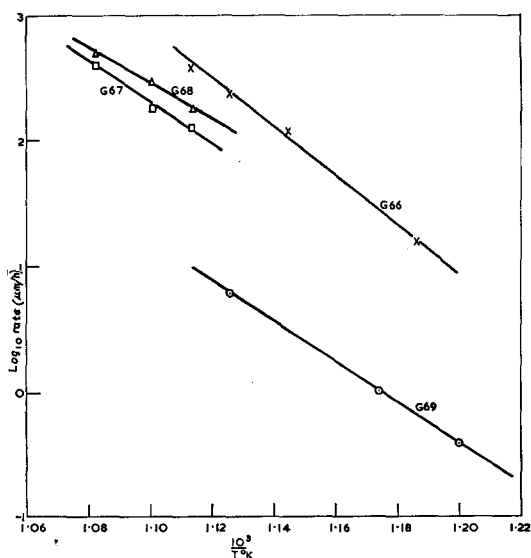
Figure 10 Arrhenius plots of crystal growth rates in G 66 to G 69. Activation energies (estimated accuracy ± 10%) G 66: 88 kcals/mole, G 67: 74 kcals/mole, G 68: 65 kcals/mole, G 69: 73 kcals/mole.

concentration of nuclei per cc was deduced from replicas of lightly etched fracture surfaces taken at low magnification (×2700) by dividing the number of dendrites per unit area by the

maximum size of crystalline regions which were common on the micrograph.

The results, expressed graphically in fig. 11, show that the maximum concentration of nuclei was produced at 535° C. At 515 and 535° C the rate of nucleation was independent of time for the first 3 h; indeed at 515° C the rate of nucleation was found to be constant even for a 16 h treatment. At 560 and 580° C the onset of crystal growth interfered with the estimation of the rate of nucleation over an extended period; values could be obtained only for the first 2 h.

3.2.6. The Internal Structure of the Dendritic and Spherulitic Crystals

The internal structure of the dendrites was deduced from transmission electron microscopy and selected area diffraction of extraction replicas. The morphology and orientation of β-eucryptite within the dendrites was most readily observed when the specimens were etched prior to replication since this treatment selectively removed the LS. Complementary examination of unetched specimens then enabled the mutual orientation of LS and β-eucryptite to be determined.

Orientation of β-eucryptite. A typical dendrite consists of parallel crystals growing along its major axis and less well-defined crystals growing at right angles. The first group will be referred

to as spinal growths and the second as fibrils. Low temperature heat-treatment favoured the formation of spinal growths whereas at higher temperatures the dendrites were dominated by the fibrillar structure. Fig. 12 shows both types of growth occurring within one dendrite at an intermediate temperature.

Electron diffraction and dark field microscopy showed that the c-axis of the β-eucryptite crystals, both in the spine and the fibrils, lay along the direction of the dendrite axis. Thus the c-axis coincided with the long dimension of the spinal growths but with a short dimension of the fibrils.
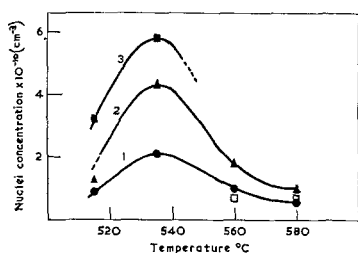
Figure 11 Nuclei per cc versus temperature in G 69 measured after 1, 2 and 3 h. Open squares represent treatments for which the onset of crystal growth interfered with evaluation of the nucleus concentration.

The most commonly observed orientation along the long axis of the fibrils, radiating away from the spine, was a β-eucryptite a-axis.

Mutual orientation of LS and β-eucryptite. Electron diffraction and dark field micrographs of extraction replicas from unetched specimens showed that the lattices of β-eucryptite and LS were usually partially coherent in the sense that the a-axis of LS and the c-axis of β-eucryptite were of equal dimension and were parallel to the dendrite axis, while in the plane normal to this the c-axis of LS coincided at least approximately in direction with one of the two-fold axes of β-eucryptite. The b-axis and the directions normal to the 011 planes of LS lay approximately along the $10\bar{1}0$ directions of β-eucryptite.

Figs. 13a and b show a typical diffraction pattern and dark field micrograph of coherent fibrils. The Moiré fringes, of separation distance 70 Å occur over considerable areas of the micrographs of the hedrite. The existence of these fringes is taken as a confirmation that the oriented relationship between LS and β-eucryptite extends over regions many times greater than that of a single fibril and hence the dendrite may be regarded as being made up of two interwoven single crystals. The distance between the fringes calculated from the dimensional mismatch
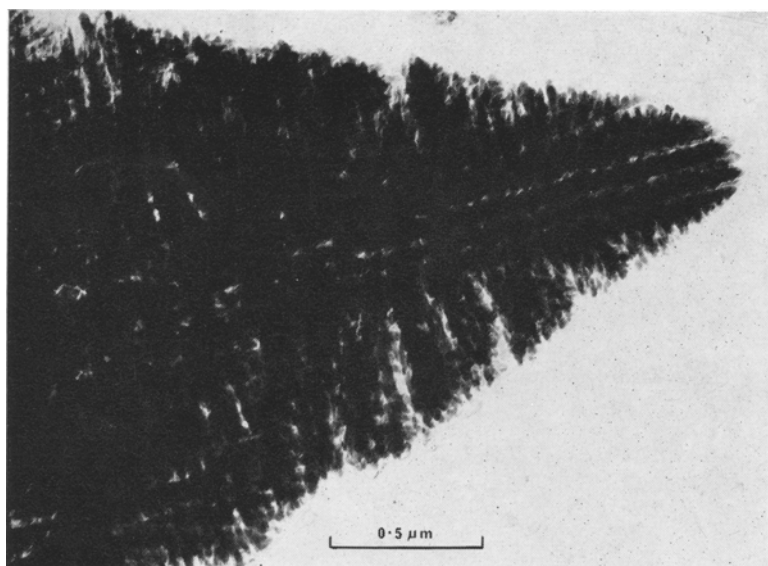
Figure 12 Extraction replica of an etched (5 secs; $\frac{1}{2}$% HF) surface of G 69 showing the β-eucryptite skeleton of a dendrite grown at 560° C having marked tendency for spinal development.

(a)

(b)
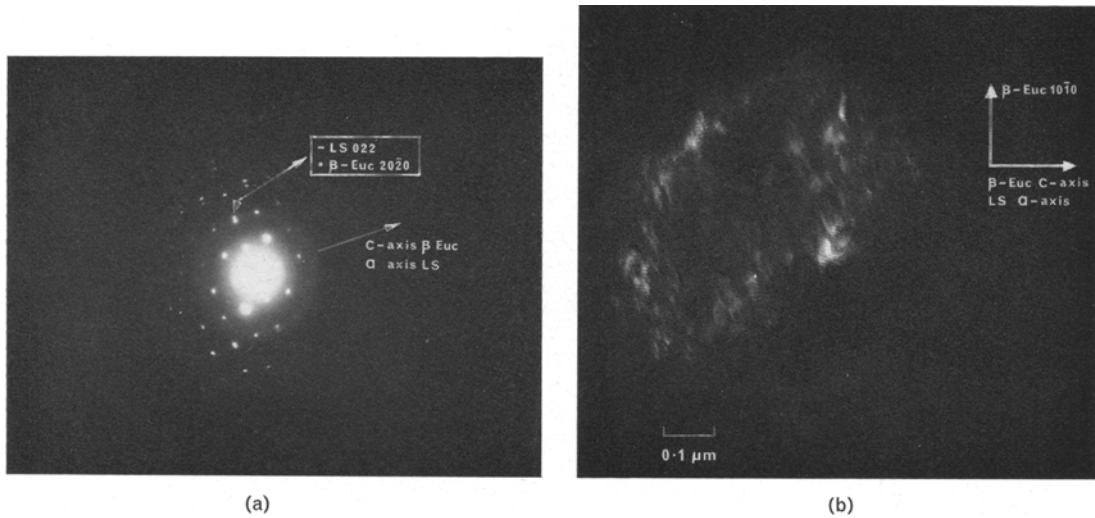
Figure 13(a) Electron diffraction pattern of part of the LS–β-eucryptite dendrite of fig.13b showing the partial coherence of the two phases. (b) Dark field electron micrograph of part of a LS–β-eucryptite hedrite showing Moiré fringes (separation 70 Å), taken with the superimposed diffracted beams from the $10\bar{1}1$ planes of β-eucryptite and 111 planes of LS. The extraction replica was taken from an unetched surface.

between the $01\,1$ spacing of LS and the $10\bar{1}0$ of β-eucryptite is in good agreement (63 Å), with that observed.

Fig. 14 illustrates the juxtaposition of the two lattices in the plane normal to the axis of coherency, i.e. normal to the dendrite axis. The data so far available do not unambiguously define the morphology of the LS or its orientation in the plane of fig. 14 with respect to the radiating fibrils; however, there are many indications that the most common orientation has the c-axis of LS and an a-axis of eucryptite along the fibrils.

Structure of the spherulites. In the spherulites
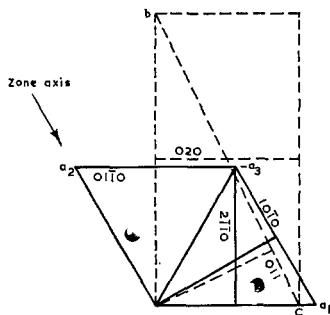
Figure 14 Orientation of LS to β-eucryptite in the plane normal to the axis of coherency.
- - - - - - - -, LS, $a = 5.43$ Å, $b = 9.41$ Å, $c = 4.66$ Å.
————, β-eucryptite, $a = 5.21$ Å, $c = 5.43$ Å.

608

the sole form of crystal growth was similar to the fibrillar growth in the dendrites (fig. 3b). This was evident from the observation of crystalline regions of mixed spherulitic and dendritic types in which there was no obvious transition from one type of fibrillar structure to another. Since the spherulites have no unique axis of symmetry, the orientations of the crystallographic axes must be randomised at least partially; however, it seems probable that the c-axis of β-eucryptite and the a-axis of LS maintain coherency and lie normal to the radial directions of the fibrils.

The origin of the internal structure. Since well-defined X-ray patterns of β-eucryptite develop in advance of those for LS it is inferred that the structure of both the spherulites and the dendrites is dictated principally by the initial growth of β-eucryptite. In the dendrites the c-axis of this phase lies along the spine, the long sides of which are bounded by $10\bar{1}0$ faces with $10\bar{1}1$ faces at the tip. This is illustrated in fig. 15.

Parallel twinning occurs along the spine to such an extent that neighbouring twinned crystals compete for nutriment from the glass. This competition restricts growth to the direction radial to the spine so that the crystals with fibrillar character are produced. It can be seen from the orientations established that the fibrils have very little surface bounded by $10\bar{1}0$ faces and much more by $10\bar{1}1$ or similar pyramidal faces.
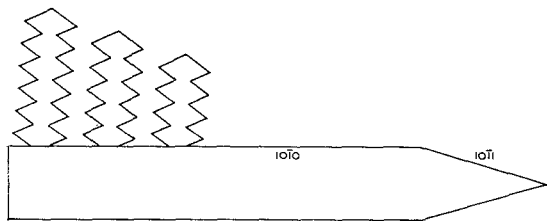
Figure 15 Schematic detail of β-eucryptite orientation in the dendrites. The fibrillar crystals are envisaged as having a large proportion of their surfaces bounded by $10\bar{1}1$ faces. The deviation from right-angled growth to the spine often occurs because the earlier growing fibrils denude the immediately surrounding glass of growth material.

At lower temperatures diffusion of the nutriment through the glass is very restricted and this leads to the twinned crystals growing closer to each other, fibrillar growth is reduced and spinal development becomes dominant.

The transition from spherulitic to dendritic growth is almost certainly caused by the thirty-fold decrease in rate of growth of the fibrils under the influence of TiO_2 (cf. section 3.2.4). The implications are that TiO_2 restricts the growth of β-eucryptite in directions normal to the $10\bar{1}0$ planes but not in those normal to the $10\bar{1}1$ faces. The slowest growing faces must have the greatest area and this leads to the elongation of the crystal and hence the formation of a spine. The implications of the relationship between dendrite morphology and the subsequent growth of LT will be taken up in the discussion. The LS appears to grow in layers between both the spinal and the fibrillar crystals. Pieces of the dendrites extracted during replication of unetched fracture surfaces showed a very marked preponderance of diffraction patterns with $hk0$ zone axes. Sections with this orientation do not intersect the strong $(SiO_3)_n$ chains and hence are likely to be easy cleavage planes. The $(SiO_3)_n$ chains lie along the c-axis of LS, and most probably along the radial directions of the dendrites. This orientation provides an explanation of why the dendrites commonly fractured radially as shown in fig. 4. The shadow contrast between the two halves of the dendrite reveals how the fracture surface has been deflected radially towards the spine.

4. Discussion

In terms of the classical theories of nucleation there are two barriers to the formation and development of stable crystals in glasses [16].

The first arises from the increase in free energy when a crystal/glass interface is formed. For a spherical nucleus this is given by

$$W^* = \frac{16\,\pi\sigma^3\,V^2}{3\,(\Delta G_V)^2},$$

σ = surface free energy/cm^2 of the crystal/glass interface; ΔG_V = change in free energy in the bulk transformation of 1 g atom from the glass to the crystal; V = g atomic volume of the crystal.

The second term is a kinetic barrier (ΔG_D) to short range diffusion or reorientation of structural units in the glass to form the ordered structure of the crystal.

From the formal expression for the rate of nucleation

$$I = n\nu e^{-(NW^*/RT)}\,e^{-(\Delta G_D/RT)},$$

where I = number of nuclei formed/cc/sec; n = number of atoms/cc; ν = vibrational frequency of atoms at nucleus/glass interface, it can be qualitatively predicted that the rate of nucleus formation will increase with decreasing temperature below the melting point, since W^* is proportional to the undercooling ΔT. It also follows that a maximum is to be expected in the I versus T curve because the second exponential term will eventually begin to predominate as T decreases, and will cause I to decrease. Both of these patterns are commonly found in studies on nucleation in glasses and are evident in this work for G 69. These expressions, developed from classical theory, cannot however predict the influence of composition and thermal history on the nucleation rate in polycomponent glasses. This difficulty arises from the intangible nature of σ, the interfacial energy, and the lack of an independent method of determining it. In addition there is not usually available a model of glass structure sufficiently detailed to enable a physical interpretation of the kinetic barrier, ΔG_D, to be made.

It is clear, however, that to promote nucleation and growth, the interfacial energy between a potential nucleus and its surroundings, and between a growing crystal and the glass matrix, must be minimised. It is in these terms that the rôle of TiO_2 as a nucleating additive is seen here. The results of the present study do not entirely support either of the commonly held views on the mechanism by which TiO_2 promotes nucleation, i.e. the creation of micro-immiscibility or primary generation of titanium-rich compounds;

609

they can however, be regarded as a justification of some of the general ideas postulated by Hillig [17]. In the remainder of this discussion some proposals will be made for an alternative mechanism [15] by which TiO_2 can be considered to be "surface active" at the boundaries of micro-domains in the glasses.

For any glass in which the ratio of oxygen ions : network forming cations is > 2 there must be non-bridging oxygen ions and a lowering of free energy would follow if chemical differentiation occurred to give domains in which the silica network were continuous and which were separated from each other by the non-bridging oxygens. Such a microstructure would provide a larger number of potential nuclei for phases whose structural elements were related to the short range order within the domains. It is postulated here that Ti^{4+} ions can create such domains by their tendency to occupy non-bridging surface sites associated with non-bridging oxygen and Li^+ ions. This tendency would be consistent with the limited ability of Ti^{4+} ions to form stable tetrahedral networks. Moreover, the rejection of the Ti^{4+} ions to the periphery would be expected, since the solubility of Ti^{4+} in the network silicate structures is very low. If it is assumed that the Ti^{4+} ions attract all the non-bridging oxygens to the surface then it can be shown that the ultimate size of the domains will be fixed for a given composition. Thus if the area occupied by a non-bridging oxygen can be assessed, then the domain size can be calculated from a knowledge of the molar ratios of ions and the volume/g atom of oxygen (derived from the density data). It is known from the crystallography of the β-quartz type structure [18] that the successive $10\bar{1}1$ planes are of area 36.6 $Å^2$ and are bridged by only two oxygen links/unit cell. The value for the area of one peripheral oxygen on the $10\bar{1}1$ plane is thus 18.3 $Å^2$ or for 1 g atom of non-bridged oxygen

$$= \frac{18.3 \times 6.02 \times 10^{23}}{10^{16}} \text{ cm}^2 = 11.0 \times 10^8 \text{ cm}^2$$

This value is assumed to be valid in the glass. To simplify the calculations, the domains, n of which contain one g atom of total oxygen, are assumed to be cubic with an edge dimension a, i.e. the volume, V, containing 1 g atom of oxygen $= na^3$ and the corresponding surface area is $6 a^2 n$.

Following Stevels [19] we can define some basic relationships: $R =$ atoms of oxygen/

network former; $Z =$ co-ordination number of network formers; $X =$ number of non-bridging oxygens per network former; $Y =$ number of bridging oxygens per network former; from which it follows

$$X + Y = Z$$
$$X + \tfrac{1}{2}Y = R$$

and the fraction of non-bridging oxygens $= X/R$

The following calculation is for G 69 in which the Ti^{4+} ions are considered to be network formers because the glass is alkali rich. $R = 188.28/80.79 = 2.33$; $X + Y = 4$; $X + \tfrac{1}{2}Y = 2.33$; therefore $X = 0.66$; therefore $Y = 3.34$ and $X/R = 0.283$. From the density, the volume/ g atom of total oxygen, $V = 12.8$ cc $= na^3$; and since $11.0 \times 10^8 \times X/R = 6a^2n$; $a = 24.3$ Å.

More detailed postulates can now be made about constitutional differences between the periphery and interior of the domains and criteria governing their stability can be proposed. The following arguments hold irrespective of the domain size actually attained in the glass. The effective negative charge already on an AlO_4 tetrahedron would make such a site energetically unfavourable for non-bridging oxygens and it therefore follows that all the Al^{3+} would reside in the interior of any domain. If it is further argued, on the basis of the crystallisation behaviour described, that the β-eucryptite structure is embryonic in the domains, then the R, X and Y values for the composition remaining after LAS_2 is subtracted, can be calculated as before. The values of X and Y are then the number of non-bridging and bridging oxygens, respectively, per network former in the peripheral regions. If it is assumed that the Si^{4+} has no more than one non-bridging oxygen and the Ti^{4+} has the rest, then for G 69 it is calculated that the O (non-bridged): Ti ratio is 1.5. A plausible general condition for stability of domains constituted in this way is that the O (non-bridged) : Ti ratio should be < 2, since for higher values the Ti^{4+} ions could readily loosen from the network and form structures of their own. Alternatively more Si^{4+} ions might migrate from the network regions and occupy the non-bridging sites. This second mechanism would have the effect of stabilising the Ti^{4+} ions but, by bringing Al^{3+} ions in closer proximity in the network regions, LA type compounds should precipitate.

The basic difference in crystallisation behaviour between G 70 and the other glasses

can be explained on the basis of these hypotheses since, for G 70, it works out that the O (non-bridged) : Ti ratio is 2.5 : 1 and hence domain instability is inherent. In this glass the primary generation of large numbers of LT crystallites (4×10^{15}/cc) suggests that the first mechanism is dominant. However, the appearance at $580°C$ of the hexagonal phase (cf. table III) implies that there is a partial operation of the second mechanism, since there is evidence for this phase being an LA type of compound.

In terms of the parameters of the classical theory of nucleation and growth, the model advanced for the action of TiO_2 is qualitatively consistent with the lowering of σ and most probably ΔG_D, since the need for long range diffusion and extensive realignments will be reduced for growth within and between localised domains.

The lowered rate of growth of the hedrites is also consistent with a model in which potential growth centres at the interface between glass and crystals are occupied by Ti^{4+} ions which must be displaced before growth can continue. The dendritic habit consequent on the addition of titania within the limit O (non-bridged) : Ti < 2, can be explained if it is assumed that the displaced Ti^{4+} ions become preferentially absorbed on the $10\bar{1}0$ faces of β-eucryptite. This retards development *normal* to the *c*-axis, whereas it is relatively unimpeded *along* the *c*-axis, i.e. in the direction of the spine of the dendrites (cf. section 3.2.6). The experimental finding that LT development is inhibited when dendrites are allowed to develop slowly by prolonged heating at lower temperatures, supports the assumption of selective absorption of Ti^{4+} ions on the β-eucryptite $10\bar{1}0$ face. The internal structure of dendrites grown in this manner differs from that of those grown more rapidly at higher temperatures (when LT co-crystallises). At the lower temperature the β-eucryptite crystallites have more of their surface composed of $10\bar{1}0$ faces which, by absorbing Ti^{4+} ions, inhibit their free migration and aggregation. These three crystallo-chemical observations give self-consistent support for the surface active rôle of titania in nucleation and crystal growth processes in these glasses.

As expected the growth units from these glasses based on eutectic compositions were internally fine-grained, but the overall microstructures were coarse and could not readily be classified into any of the standard categories of eutectic microstructures [20]. The polycrystalline materials were disappointingly weak. Although the reasons for mechanical failure in glass-ceramics are still not fully understood, it seems probable in the present case that the deformations and stresses arise either from the change in volume on crystallisation or the thermal expansion mismatch between the phases. Stress relief could be achieved only with smaller growth units, which would require a higher nucleation density than has been achieved with the chosen compositions.

5. Conclusions

(i) In the glasses studied, titanium dioxide does not promote nucleation either by inducing gross glass-in-glass separation or by epitaxial growth on lithium titanate crystallites.

(ii) Ti^{4+} ions cause a redistribution of non-bridging oxygen ions to the periphery of completely bridged network regions and in this sense function as a surface active agent.

(iii) Ti^{4+} ions modify the kinetics and morphology of crystal growth by becoming preferentially sited on particular crystal faces of β-eucryptite.

(iv) Clear evidence is presented for oriented relationships between the phases co-crystallising within the growth units.

References
1. P. W. MCMILLAN, "Glass Ceramics" (Academic Press, London, 1964) p. 113.
2. V. V. VARGIN, "Catalyzed Controlled Crystallisation of Glasses in the Lithium Aluminosilicate System" (Khimiya Press, Leningrad, 1964), (Consultants Bureau, New York, 1965).
3. N. A. TOROPOV and V. P. BARZAKOVSKII, "High Temperature Chemistry of Silicates" (Consultants Bureau, New York, 1966), p. 15.
4. S. O. STOOKEY, Glastech. Ber. 32K (1959) V/1.
5. R. ROY, J. Amer. Ceram. Soc. 43 (1960) 670.
6. E. V. PODUSHKO and A. B. KOZLOVA, "Catalyzed Crystallisation of Glass", Vol. 3, edited by E. A. Porai-Koshits (Academy of Sciences Press, Leningrad, 1963), (Consultants Bureau, New York, 1964), p. 77.
7. "Symposium on Nucleation and Crystallisation in Glasses and Melts", edited by M. K. Reser (American Ceramic Society, 1962).
8. R. D. MAURER, J. Appl. Phys. 33 (1962) 2132.
9. R. ROY and E. F. OSBORN, J. Amer. Chem. Soc. 71 (1949) 2086.
10. M. KRISHNA MURTHY and F. A. HUMMEL, J. Amer. Ceram. Soc. 37 (1954) 14.
11. K. A. JACKSON and J. D. HUNT, Trans. Met. Soc. AIME 236 (1966) 843 and 1129.
12. R. P. MILLER and G. SOMMER, J. Sci. Instr. 43 (1966) 293.

13. M. MAREZIO, *Acta Cryst.* **19** (1965) 396.
14. P. H. GEIL, "Polymer Single Crystals" (J. Wiley, New York, 1963).
15. T. I. BARRY and L. A. LAY, "6th Intern. Symp. Reactivity of Solids" Schenectady (1968) (J. Wiley, New York, 1969).
16. D. TURNBULL and M. H. COHEN, "Modern Aspects of the Vitreous State", Vol. 1, edited by J. D. Mackenzie (Butterworths, London, 1960) p. 38.

17. W. B. HILLIG [7] p. 77.
18. H. G. F. WINKLER, *Acta Cryst.* **1** (1948) 27.
19. J. M. STEVELS, "Handbuch der Physik", vol. 20, edited by S. Flüggge (Springer-Verlag, Berlin, 1957) p. 350.
20. J. A. CHADWICK, *Prog. Mat. Sci.* **12** (1963) No. 2.